厚生労働科学研究費補助金

トキシコゲノミクス研究事業

# トキシコゲノミクスのための遺伝子ネットワーク解析法の開発

平成１８年度　総括研究報告書

主任研究者　奥野　恭史

平成１９（２００７年）　４月

# 目　次

厚生労働科学研究費補助金（トキシコゲノミクス研究事業）
総括研究報告書

# トキシコゲノミクスのための遺伝子ネットワーク解析法の開発

主任研究者　奥野　恭史　京都大学薬学研究科 助教授

研究要旨
本研究は、化合物による生体系への影響を、薬物作用遺伝子群や毒性関連遺伝子群の遺伝子発現ネットワーク（分子ネットワーク）の変動として解析する高精度な薬物安全評価アルゴリズムの開発と実用化を目的としている。すなわち、化合物を作用させた各種細胞のDNA マイクロアレイ実験による網羅的遺伝子発現データから、バイオインフォマティクス手法によって薬物毒性特有の遺伝子発現ネットワークを構築し、薬物毒性を反映する遺伝子ネットワークのパターンとして薬物安全性を評価するトキシコゲノミクス計算法の確立を目指す。一般に遺伝子発現ネットワーク解析手法は、生命現象と分子メカニズムを繋げる有力なバイオインフォマティクス手法であり、本手法をトキシコゲノミクスへ適用することにより毒性と遺伝子発現パターンの相関を鮮明にし、予測精度の向上と毒性分子メカニズムの解明という成果をもたらすものと予想される。近年、マイクロアレイ解析のトキシコゲノミクスや薬理ゲノミクスへの適用に対する期待が国内外を問わず高まって来ているが、トキシコゲノミクスや薬理ゲノミクスへのネットワーク解析手法の適用・成功事例は今のところ世界的に皆無である。従って、本研究は、ネットワーク解析法のトキシコゲノミクスへの応用という試み自身の独創性を有しており、薬物の毒性評価とその毒性発現の分子メカニズムに関する知見をも同時に提供する強い特色を有している。2年次にあたる平成18年度の研究進捗も、計画通り極めて順調に進捗した。具体的には、薬物毒性を評価する上で最も重要な組織である肝臓における薬物毒性の分子メカニズムを解明するため、ヒト肝癌由来細胞株であるHepG2細胞を用いて、肝毒性を有するインスリン抵抗性改善薬トログリタゾン(TGZ)に加えて、同じチアゾリジン系抗糖尿病薬物であるが肝毒性が少ないとされるピオグリタゾン(PGZ)で刺激させた際の経時的な網羅的遺伝子発現データの追加実験収集を行い、遺伝子ネットワークの構築及び解析を行った。その結果、トログリタゾンの薬物細胞毒性に特異的な遺伝子ネットワーククラスターを見いだし、その中に含まれる遺伝子群の同定に成功した。本研究によって開発される高精度な毒性予測手法は、医薬品開発における早期毒性予測による医薬品開発期間・コストの軽減化と、国民における医薬品使用の安全性の向上を実現するものと期待できる。

## A．研究目的

ポストゲノム時代の今日、生命科学研究の関心は遺伝子・蛋白質の単一の機能解明にとどまらず、これらを統合した生命システム全体の機能解明へと移行しつつある。医薬の観点においても、化合物と直接作用する単一のタンパク(遺伝子）の機能変化からその薬理活性の全てを語り尽くそうとする従来の考え方では不十分であり、化合物と特定のタンパク質との直接的な作用が周辺や下流の遺伝子たちにどのような影響を及ぼすのかという化合物と生体系との作用を多種多様な生命システムの変動とみなす新しい概念の導入および解析法の開発が必須である。そこで、本研究は、薬物標的分子や毒性原因遺伝子などの単一遺伝子(タンパク質）を対象にした従来の解析手法から逸脱し、化合物による生体系への影響を薬物作用遺伝子群や毒性関連遺伝子群の遺伝子発現ネットワークの変動として解析する高精度な薬物安全評価アルゴリズムの開発と実用化を目的としている。すなわち、薬物曝露におけるマイクロアレイ実験による網羅的遺伝子発現データから、バイオインフォマティクス手法によって薬物毒性特有の遺伝子発現ネットワークを構築し、薬物毒性を反映する遺伝子ネットワークのパターンとして薬物安全性を評価するトキシコゲノミクス計算法の確立を目指す。一般に遺伝子発現ネットワーク解析手法は、生命現象と分子メカニズムを繋げる有力なバイオインフォマティクス手法であり、本手法をトキシコゲノミクスへ適用することにより毒性と遺伝子発現パターンの相関を鮮明にし、予測精度の向上と毒性分子メカニズムの解明という成果をもたらすものと予想される。研究計画としては、初年度（平成17年度）にはアルゴリズム開発のための実験データを収集し、2 年次（平成18年度）にはアルゴリズムの実質的開発と追加マイクロアレイ実験を行い、最終年度となる平成19年度には、先の2年間で開発検討行ってきたネットワーク解析手法の有効性の評価とそれによる改良、汎用化を目指す。最終的には、マイクロアレイデータを入力とした時に、薬理作用遺伝子ネットワーク、毒性作用遺伝子ネットワークを自動抽出し、その薬理効果・毒性作用を予測するシステムとする。本研究によって開発される高精度な毒性予測手法は、医薬品開発における早期毒性予測による医薬品開発期間・コストの軽減化と、国民における医薬品使用の安全性の向上を実現するものと期待できる。

## B．研究方法

### 1.チアゾリジン系薬物投与下での肝毒性評価系の構築とマイクロアレイ実験データの収集

[細胞培養]：10% (v/v) fetal bovine serum (GIBCO)、100 U/mL penicillin (GIBCO) および100 µg/mL streptomycin (GIBCO) を含有するDulbecco's Modified Eagle Medium (GIBCO) を用い、コラーゲンコートディッシュにて37℃、5% CO2の条件で細胞培養を行った。

[WST-1細胞増殖測定]：WST-1を基質としたNADH (Nicotinamide adenine dinucleotide) 還元酵素の活性を指標に、細胞増殖を測定した。HepG2細胞1x104 cellsをvehicle (1% dimethylsulfoxide)及び各濃度 (3 µM, 100 µM) のトログリタゾンもしくはピオグリタゾンで刺激し、各０，２，６，１２，２４時間後に飽和WST-1溶液 (Roche) を加えた。37℃、5 % C

02の条件下で2時間反応させた後、還元型WST-1（Formazan）の増加量を測定するため、マイクロプレートリーダーで460nmの吸光度を測定した。さらに、バックグラウンドシグナルとして650nmの吸光度を測定した。

[マイクロアレイ解析]：vehicle及び各濃度（3 μM, 100 μM）のトログリタゾンもしくはピオグリタゾンで刺激したHepG2細胞を、刺激後０，２，６，１２，２４時間後にそれぞれ回収し、acid guanidiniumthiocyanate-phenol-chloroform法ならびにRneasy mini kit（Qiagen）を用いてtotal RNAを抽出・精製した。これにT7- $dT_{24}$ プライマーをアニールさせ、1st strand DNAを合成し、引き続いて2nd strand DNAを合成した。この二本鎖DNAを鋳型として、T7 RNA ポリメラーゼによりビオチン標識dNTPを用いてビオチン標識antisense RNAを合成した。このantisense RNAを200塩基以下に断片化し、Human Genome U133 Plus 2.0 Array (Affymetrix)にハイブリダイゼーションした。１６時間後、ストレプトアビジン－フィコエリスリンにて蛍光ラベル化を行い、Genome U133 Plus 2.0 Arrayの蛍光イメージを取得した。

## ２．チアゾリジン系薬物作用遺伝子ネットワークの構築

トログリタゾンとピオグリタゾンのマイクロアレイデータにおいて、各濃度の時系列において発現量が３倍以上変動した遺伝子を抽出した。全濃度での時系列における発現変動パターンに基づいてクラスタリングした後に濃度毎に分割する事により、各薬剤及び各濃度の遺伝子ネットワークと薬剤及び濃度間での遺伝子ネットワークの構築を行った。遺伝子の経時的な発現パターンが薬物刺激によってどの様な変動を受けるのかを分類する為、3倍以上変動している遺伝子群の発現変動プロファイルについて、k-means 法で120種類のクラスターに分類した。

次に、各クラスター内の代表的な遺伝子変動パターンを得るため、各クラスターのベクトル重心

$V_{CL=n}=(v_{t=0h},v_{t=2h}^{C=0},\cdots,v_{t=24h}^{C=0},v_{t=2h}^{C=3},\cdots,v_{t=24h}^{C=3},v_{t=2h}^{C=100},\cdots,v_{t=24h}^{C=100})$

を計算し、濃度C=(vehicle;0μM, 3μM, 100μM)毎のベクトル$V_{CL=n}^{C=m}$,

$(n=1,\cdots,120, m=0,3,100)$に分割した。このとき、クラスター重心は薬物毎に計算した。さらに、クラスターを固定し、各濃度間(C=0 vs C=3, C=0 vs C=100, C=3 vs C=100）での相関係数 $CC_{CL=n}^{C=(m_i,m_j)}=Cov(V_{CL=n}^{C=m_i},V_{CL=n}^{C=m_j})$,

$(i\neq j)$を計算し、次に、濃度を固定し各クラスター重心の相関係数

$CC_{CL=(n_k,n_l)}^{C=(m_i,m_j)}=Cov(V_{CL=n_k}^{C=m_i},V_{CL=n_l}^{C=m_j})$, $(k\neq l)$を計算した。「120クラスター」×「3濃度」のクラスター間相関を距離として主座標分析法により座標を決定し、遺伝子ネットワーク及び変動パターンの変化を図示した。さらに、分類された遺伝子クラスターから毒性特異的なノードを抽出するため、前記の1,428個の遺伝子に対する主成分分析を行い、その結果をクラスターに反映させた。

なお、本研究は計算機アルゴリズムの開発と培養細胞を用いたインビトロ実験のみであり、倫理面に関する問題は一切無い。

## Ｃ．研究結果

### 1.チアゾリジン系薬物投与下での肝毒性評価系の構築とマイクロアレイ実験データの収集

本研究では、まず肝臓における薬物毒性発現の分子メカニズムを明らかにするため、肝毒性を有する薬物として劇症肝炎などの肝障害

を引き起こしたため臨床での使用が中止されたトログリタゾン、肝毒性の予測を目的としたモデルとしてヒト肝癌由来細胞株HepG2を用いて解析を行った。また、肝毒性のネガティブコントロールとして、トログリタゾンと同じくperoxisome-proliferator activated receptor gamma (PPARγ)のリガンドであり、チアゾリジン骨格を有するインスリン抵抗性改善薬であるが、肝毒性が少ないとされているピオグリタゾンを用いた。

トログリタゾンのHepG2細胞に対する毒性用量を確認するため、WST-1法を用いてトログリタゾンとピオグリタゾンがHepG2細胞の増殖に及ぼす影響を調べた (Figure 1)。その結果、vehicleと比較してトログリタゾン100 μM刺激群において、刺激後6時間から有意な増殖の抑制が検出され、刺激後２４時間において最も顕著な増殖抑制効果が検出された。一方、トログリタゾン3 μMやピオグリタゾン刺激群では増殖抑制作用は検出されず、むしろピオグリタゾン刺激後２４時間においては増殖の亢進が検出された。ピオグリタゾンによるHepG2細胞の増殖促進作用に関して、3 μMと100 μMの濃度における差は検出されなかった。以上のこととPPARγに対するトログリタゾンとピオグリタゾンのEC50から、HepG2細胞に対するトログリタゾンの毒性用量としては100 μM、薬効(非毒性)用量としては3 μMと定義し、以後の解析を行った。

vehicle及び各濃度 (3 μM, 100 μM) のトログリタゾンもしくはピオグリタゾンで刺激したHepG2細胞の０，２，６，１２，２４時間後における経時的なマイクロアレイデータの収集を行った。各薬物刺激０時間と２４時間後における全遺伝子のシグナル値を比較したところ、他に比べ、毒性用量であるトログリタゾン100 μMにおいて発現変動の度合いが大きいことが示唆された(Figure 2)。また、トログリタゾンとピオグリタゾンのマイクロアレイデータにおいて、各濃度の時系列において発現量が３倍以上変動した遺伝子を抽出したところ、Figure 2の結果と同様に、トログリタゾン100 μMにおいて発現変動している遺伝子の数が顕著に多いことが明らかとなった(Figure 3)。

## ２.チアゾリジン系薬物作用遺伝子ネットワークの構築

そこで、Figure 3において抽出された合計1,428個の遺伝子において遺伝子ネットワークの構築を行い、薬物及び薬物濃度間における遺伝子ネットワークの変動を解析した(Figure 4)。「120クラスター」×「3濃度」のクラスター間相関を距離として主座標分析法により座標を決定し、遺伝子ネットワーク及び変動パターンの変化を図示した。各層でのxy平面内での距離は、クラスター間相関を反映しているため、近接しているクラスター同士は類似した変動パターンを持っており、各層間での移動が大きいクラスターは、濃度間での発現変動量が大きい事を示している。各薬剤において特異的な遺伝子のみを含むクラスターから薬剤特異的ネットワークを、遺伝子が両薬剤で発現するクラスターから共通ネットワークを構成した結果、トログリタゾンもしくはピオグリタゾンに特異的な変動を示すクラスター群と、トログリタゾンとピオグリタゾンで共通した変動を示すクラスター群が同定された(Figure 4)。

これらのクラスターからトログリタゾンによる細胞毒性に大きく寄与するクラスターを選定するため、前記の1,428個の遺伝子に対する主成分分析を行い(Figure 5)、その結果をクラスターに反映させた(Table 1)。トログリタゾンおよびピオグリタゾンの全濃度の経時的発現変動に対して主成分分析を行い、3変数に

情報を集約したところ、第二主成分においてトログリタゾン毒性濃度である100μMで刺激した際のベクトルとそれ以外の濃度で刺激した際のベクトルが逆の方向性を示した。従って、第二主成分はトログリタゾンによる毒性を示していると判断された(Figure 5)。次に、第二主成分スコアの上位および下位それぞれ１００位以内に含まれる遺伝子を多く含むクラスターを選別した(Table 1)。その結果からトログリタゾンの毒性発現に寄与すると予測された遺伝子を多く含み、トログリタゾンの毒性発現に特異的な発現変動パターンを提示するクラスターとして、クラスター２０(CL20)及び１２(CL12)などが選定された。トログリタゾン特異的なCL20及びCL12はvehicle及び3μMでは殆ど変動が見られないが、100μMにおいてネットワーク上での位置が大きく変動していた(Figure 6)。

## D．考察

HepG2細胞とトログリタゾン及びピオグリタゾンを用いた遺伝子ネットワーク解析を行い、主成分分析結果を反映させた結果、トログリタゾンの薬物細胞毒性に特異的なクラスターが同定された(Table 1)。主成分分析のみでは、高変動を示す遺伝子のみが選別され、それ以外の重要な働きを持つ遺伝子群は見落とされる傾向にあるが、本手法では、毒性特異的な主成分の上位／下位の遺伝子を多く含む薬物毒性特異的変動クラスターを選別する事により、薬物毒性特異的に変動したクラスター（遺伝子群）として同定することが可能となった。これらのクラスターには、アポトーシスの感受性に関わる遺伝子や細胞周期に関わる遺伝子に加えて、細胞毒性とは関連がまったく報告されていない酵素類や細胞外マトリックス因子も含まれており、たいへん興味深い。主成分分析第二主成分における遺伝子順位や遺伝子発現変動の度合いから、まずはCL20及びCL12に注目し、CL20及びCL12に含まれる遺伝子群がシステムとして薬物毒性に寄与しているかどうかを、クラスターに含まれる遺伝子群の遺伝子産物に対する活性化剤および抑制剤の処理や、上記の遺伝子群の過剰発現やsiRNAによる発現低下を行うことで、生物学的に検証する予定である。

## E．結論

### 1.チアゾリジン系薬物投与下での肝毒性評価系の構築とマイクロアレイ実験データの収集

薬物毒性を評価する上で最も重要な組織である肝臓における薬物毒性の分子メカニズムを解明するため、ヒト肝癌由来細胞株であるHepG2細胞を用いて、肝毒性を有するインスリン抵抗性改善薬トログリタゾン(TGZ)に加えて、同じチアゾリジン系抗糖尿病薬物であるが肝毒性が少ないとされるピオグリタゾン(PGZ)で刺激させた際の経時的な網羅的遺伝子発現データの追加収集を行った。

### 2.チアゾリジン系薬物作用遺伝子ネットワークの構築

遺伝子ネットワーク構築手法として、相関係数ネットワークを適用し、薬物非投与時の遺伝子ネットワーク、トログリタゾン・ピオグリタゾンそれぞれの薬物投与時（３μM、100μM）の遺伝子ネットワークを構築した。これにより、トログリタゾンの薬物細胞毒性に特異的な遺伝子ネットワーククラスターを見いだし、その中に含まれる遺伝子群の同定に成功した。

## F．健康危険情報

特記事項無し

## G．研究発表

### 1．論文発表

1. Naito, Y., Takematsu, H., Koyama, S., Miyake, S., Yamamoto, H., Fujinawa, R., Sugai, M., Okuno, Y., Tsujimoto, G., Yamaji, T., Hashimoto, Y., Itohara, S., Kawasaki, T., Suzuki, A., Kozutsumi, Y., "Germinal center marker GL7 probes activation-dependent repression of N-glycolylneuraminic acid, a sialic acid species involved in the negative modulation of B cell activation." Mol. Cell Biol., 27(8), 3008-22, 2007.
2. Osada, S., Naganawa, A., Misonou, M., Tsuchiya, S., Tamba, S., Okuno, Y., Nishikawa, J., Satoh, K., Imagawa, I., Tsujimoto, G., Sugimoto, Y., and Nishihara, T. "Altered gene expression of transcriptional regulatory factors in tumor marker-positive cells during chemically induced hepato--carcinogenesis." Toxicology Letters, 167, 106-113, 2006
3. Tsuchiya, S., Okuno, Y., Tsujimoto, G. "MicroRNA: biogenetic and functional mechanisms and involvements in cell differentiation and cancer.", J. Pharmacol. Sci., 101(4):267-70, 2006
4. Okuno, Y., Yang, J., Taneishi, K., Yabuuchi, H., Tsujimoto, G., "GLIDA: GPCR-Ligand database for Chemical Genomic Drug Discovery" Nucleic Acids Research, 34, D673-7, 2006

### 2．学会発表

1. 日本薬物動態学会 第21回年会「ケミカルゲノミクスからの創薬インフォマティクス」2006年12月1日
2. 第32回情報処理技術検討交換会「ケミカルゲノミクス情報のデータマイニング」2006年11月30日
3. モレキュラーライブラリー研究会「ケミカルゲノミクス情報を用いた化合物ライブラリーの合理的設計」2006年11月16日
4. 第34回構造活性相関シンポジウム奨励講演「ケミカルゲノミクス情報に基づく化合物探索」2006年11月14日
5. 第269回ＣＢＩ学会「ケミカルゲノム情報に基づくGPCR創薬」2006年11月1日
6. 第21回21世紀の薬学を探る京都シンポジウム - 薬学教育フロンティア -「インフォーマティクスと創薬」2006年10月14日
7. 第２回バイオメディカル研究会「ケミカルゲノミクスのための創薬インフォマティクス」2006年9月12日
8. 第４回先端医療セミナー「ケミカルゲノミクスからのIn silico創薬」2006年8月25日
9. 第45回バイオグリッドビジネスサロン「創薬におけるバイオインフォマティクスの可能性」2006年8月18日
10. 第16回近畿バイオインダストリー振興会議　技術シーズ公開会「創薬リード化合物自動合成装置の研究開発」2006年7月28日
11. コンピュータ化学部会 平成18年度例会「ケミカルゲノム情報に基づくIn silico創薬」2006年6月13日

12. バイオグリッド研究会 － ITプログラム成果報告と今後の展開 －「化合物空間を利用した化合物検索」2006年5月27日
13. （財）サントリー生物有機科学研究所　コロキウム「ケミカルゲノミクスのためのインフォマティクス」2006年2月21日

## H. 知的財産権の出願・登録状況（予定も含む）

１．特許取得

1. 特願２００７－５３３２２、「マイクロＲＮＡ標的遺伝子予測装置」、平成１９年３月２日出願、出願人　東レ株式会社、発明者　奥野恭史、辻本豪三、国本亮、寺澤和哉、土屋創健、秋山英雄、妙本明
2. 公開番号ＷＯ２００７／００４４７９　Ａ１（特開２００７－１１７５２）、「データ処理装置、データ処理プログラム、それを格納したコンピュータ読み取り可能な記録媒体、およびデータ処理方法」、平成１９年１月１１日公開、出願人　京都大学、発明者　奥野恭史、辻本豪三、梁智允、種石慶
3. 特願２００６－１４７４３３、「ケミカルゲノム情報に基づく、タンパク質－化合物相互作用の予測と化合物ライブラリーの合理的設計」、平成１８年５月２６日出願、出願人　京都大学、発明者　奥野恭史、種石慶、辻本豪三

２．実用新案登録

無し

３．その他

無し

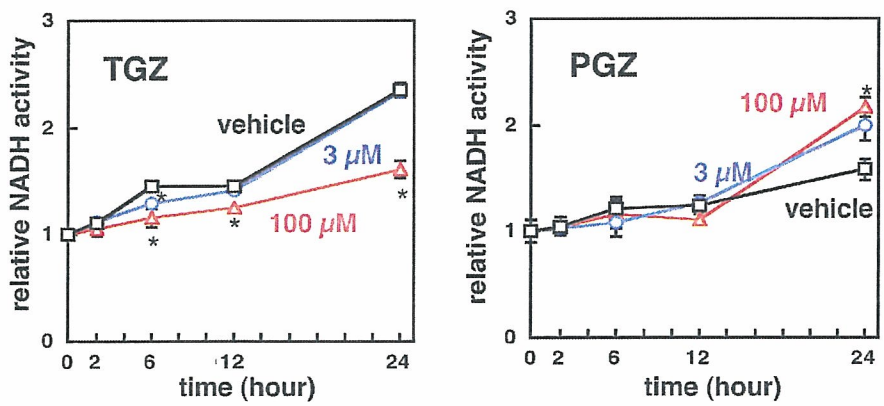


Figure 1. The effect of TGZ and PGZ on cell growth of HepG2 cells. HepG2 cells were stimulated with vehicle (black, □; 0.1% dimethylsulfoxide), 3 μM (black, ○), or 100 μM(red, △) TGZ or PGZ for the indicated times. Data are shown as the mean ± SEM (n = 3). Data are represented as fold of the value at 0 h. The data are a representative of three similar experiments (*, $p < 0.05$ for TGZ or PGZ vs vehicle).

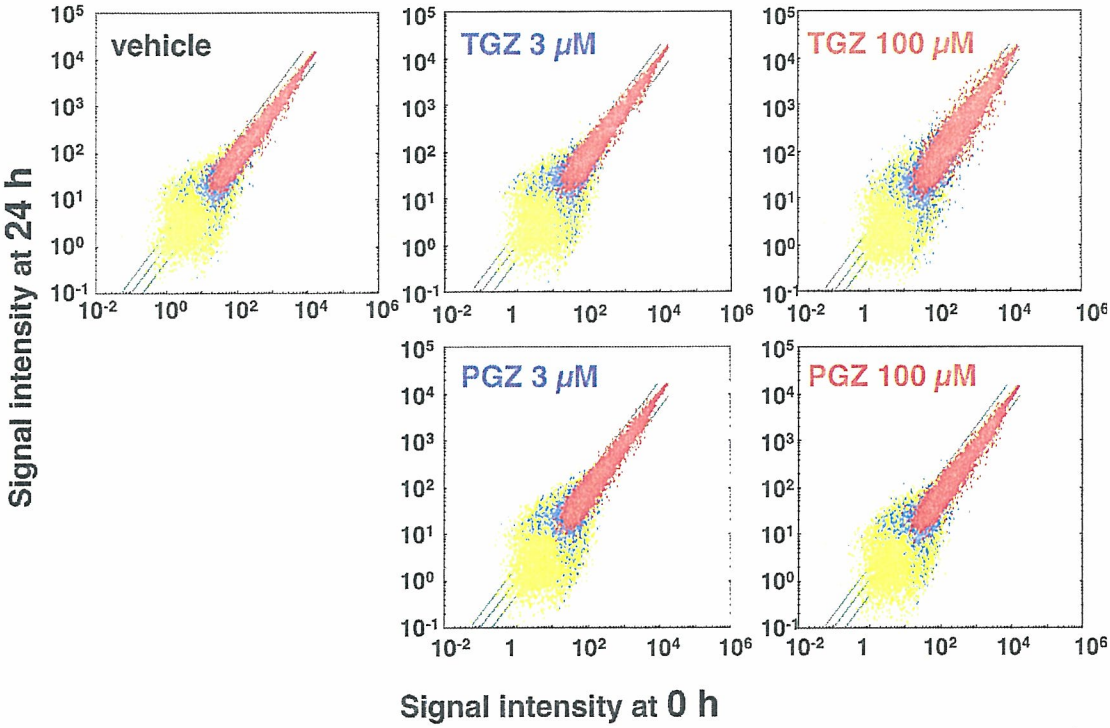


Figure 2. Scatter correlation graph representing the expression levels of genes at 0 h and 24 h in TGZ- or PGZ-treated HepG2 cells. For each gene, the expression level at 0 h is given on the X axis, and the expression level for the same gene at 24 h is plotted on the Y axis. Red dots show genes judged as "Presence", and yellow dots represent genes judged as "Absence" by GeneChip Operating Software (GCOS) of Affymetrix in both microarray analyses. Blue dots show genes judged as "Presence" only in either microarray analysis. The same and two-fold induction and suppression thresholds were indicated as diagonal lines.

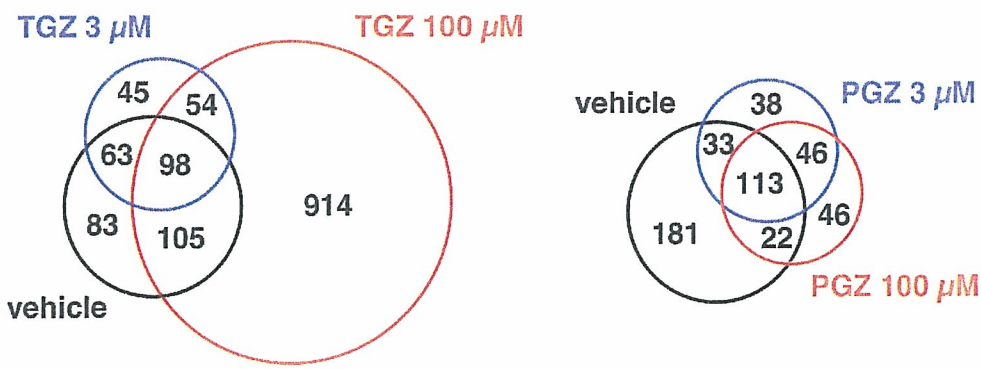


Figure 3. Overlapping sets of genes differently expressed in each concentration of TGZ or PGZ. Numbers in the overlapping region of the Venn diagram represent shared genes. Genes were selected if the ratio of the relative expression level in time course was larger or smaller than 3.0.

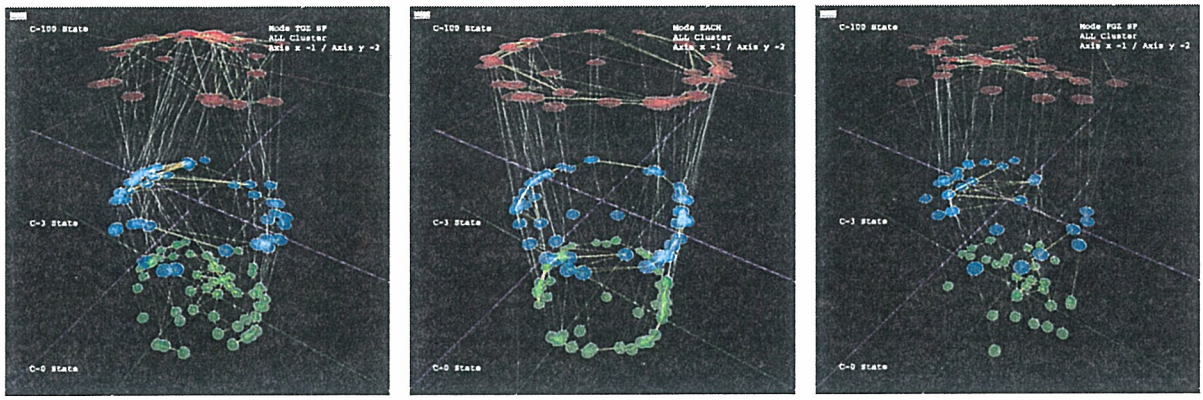

Figure 4. Genes networks by the stimulation of TGZ and PGZ in HepG2 cells. The TGZ-specific n etwork (left panel), PGZ-specific network (right panel) and the network common between TGZ an d PGZ (middle panel) were displayed.

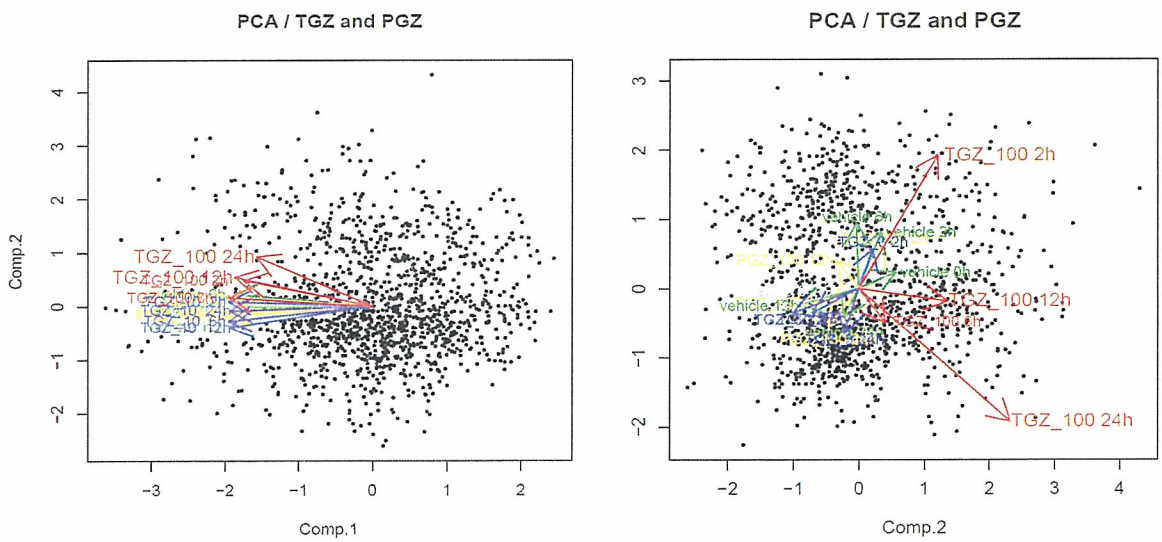


Figure 5. Principal component analysis of gene expression profiles in TGZ- or PGS-stimulated HepG2 cells. Genes were selected if the ratio of the relative expression level in time cours e was larger or smaller than 3.0. The axes correspond to principal component (Comp.) 1, Comp. 2 and Comp.3. Red arrows represent vectors of 100 μM TGZ-stimulated samples, and other color arrows represent samples except for TGZ 100 μM.

Table 1. Relation between the principal component analysis and each cluster of genes network.

| Cluster Number | Number of genes | | |
|---|---|---|---|
| | PCA (Comp. 2) | TGZ | PGZ |
| *Upper 100 genes of Comp. 2* | | | |
| *39* | *18* | *29* | *1* |
| *82* | *17* | *3* | *31* |
| *20* | *11* | *18* | *0* |
| *59* | *10* | *19* | *0* |
| *51* | *10* | *11* | *0* |
| *Lower 100 genes of Comp. 2* | | | |
| *12* | *30* | *36* | *0* |
| *50* | *14* | *1* | *33* |
| *21* | *13* | *10* | *26* |
| *25* | *12* | *15* | *0* |
| *49* | *10* | *11* | *0* |
| *11* | *10* | *0* | *25* |

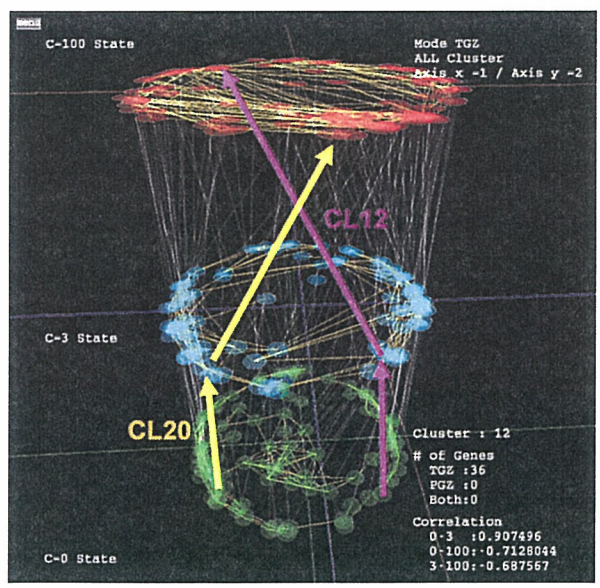


Figure 6. CL20 and CL12 in the genes network of TGZ-stimulated HepG2 cells.

研究成果の刊行に関する一覧表

書籍

| 著者氏名 | 書籍全体の編集者名 | 書籍名 | 出版社名 | 出版地 | 出版年 |
|---|---|---|---|---|---|
| 奥野恭史ほか | 日本バイオインフォマティクス学会 | バイオインフォマティクス事典 | 共立出版㈱ | 日本 | 2006 |
| 奥野恭史ほか | 石渡信一・桂勲・桐野豊・美宅成樹 | 生物物理学ハンドブック | ㈱朝倉書店 | 日本 | 2007/4/20刊行予定 |

雑誌

| 発表者氏名 | 論文タイトル名 | 発表誌名 | 巻号 | ページ | 出版年 |
|---|---|---|---|---|---|
| Naito, Y., Takematsu, H., Koyama, S., Miyake, S., Yamamoto, H., Fujinawa, R., Sugai, M., Okuno, Y., Tsujimoto, G., Yamaji, T., Hashimoto, Y., Itohara, S., Kawasaki, T., Suzuki, A., Kozutsumi, Y. | Germinal center marker GL7 probes activation-dependent repression of N-glycolylneuraminic acid, a sialic acid species involved in the negative modulation of B cell activation. | **Mol. Cell Biol.** | 27(8) | 3008-22 | 2007 |
| Osada, S., Naganawa, A., Misonou, M., Tsuchiya, S., Tamba, S., Okuno, Y., Nishikawa, J., Satoh, K., Imagawa, I., Tsujimoto, G., Sugimoto, Y., and Nishihara, T. | Altered gene expression of transcriptional regulatory factors in tumor marker-positive cells during chemically induced hepatocarcinogenesis. | **Toxicology Letters** | 167 | 106-113 | 2006 |
| Tsuchiya, S., Okuno, Y., Tsujimoto, G. | MicroRNA: biogenetic and functional mechanisms and involvements in cell differentiation and cancer. | **J Pharmacol Sci** | 101(4) | 267-70 | 2006 |
| Okuno, Y., Yang, J., Taneishi, K., Yabuuchi, H., Tsujimoto, G. | GLIDA: GPCR-Ligand database for Chemical Genomic Drug Discovery | **Nucleic Acids Research** | 34 | D673-7 | 2006 |

その他

| 著者氏名 | 執筆タイトル名 | 掲載誌名 | 巻号 | ページ | 出版年 |
|---|---|---|---|---|---|
| 奥野　恭史ほか | ケミカル・バイオ情報に基づく創薬インフォマティクス研究 | Pharma VISION NEWS | No. 9 | 13-16 | 2007 |
| 日刊工業新聞　2007. 3. 26　掲載記事 | | | | | |

研究成果の刊行物・別刷

MOLECULAR AND CELLULAR BIOLOGY, Apr. 2007, p. 3008–3022 Vol. 27, No. 8
0270-7306/07/$08.00+0 doi:10.1128/MCB.02047-06


# Germinal Center Marker GL7 Probes Activation-Dependent Repression of *N*-Glycolylneuraminic Acid, a Sialic Acid Species Involved in the Negative Modulation of B-Cell Activation▽†

Yuko Naito,[1,7] Hiromu Takematsu,[1,7] Susumu Koyama,[2] Shizu Miyake,[2] Harumi Yamamoto,[5] Reiko Fujinawa,[5] Manabu Sugai,[4] Yasushi Okuno,[3] Gozoh Tsujimoto,[3] Toshiyuki Yamaji,[5] Yasuhiro Hashimoto,[5,7] Shigeyoshi Itohara,[6] Toshisuke Kawasaki,[2]‡ Akemi Suzuki,[5] and Yasunori Kozutsumi[1,5,7]*

*Laboratory of Membrane Biochemistry and Biophysics, Graduate School of Biostudies,[1] Department of Biological Chemistry,[2] and Department of Genomic Drug Discovery, Graduate School of Pharmaceutical Sciences,[3] and Center for Genomic Medicine, Graduate School of Medicine,[4] Kyoto University, Sakyo, Kyoto 606-8501, Japan; Supra-Biomolecular System Research Group, RIKEN Frontier Research System,[5] and Laboratory for Behavioral Genetics, RIKEN Brain Science Institute,[6] RIKEN, Wako, Saitama 351-0198, Japan; and CREST, Japan Science and Technology, Kawaguchi, Saitama, Japan[7]*

Received 2 November 2006/Returned for modification 9 January 2007/Accepted 30 January 2007

**Sialic acid (Sia) is a family of acidic nine-carbon sugars that occupies the nonreducing terminus of glycan chains. Diversity of Sia is achieved by variation in the linkage to the underlying sugar and modification of the Sia molecule. Here we identified Sia-dependent epitope specificity for GL7, a rat monoclonal antibody, to probe germinal centers upon T cell-dependent immunity. GL7 recognizes sialylated glycan(s), the α2,6-linked *N*-acetylneuraminic acid (Neu5Ac) on a lactosamine glycan chain(s), in both Sia modification- and Sia linkage-dependent manners. In mouse germinal center B cells, the expression of the GL7 epitope was upregulated due to the in situ repression of CMP-Neu5Ac hydroxylase (Cmah), the enzyme responsible for Sia modification of Neu5Ac to Neu5Gc. Such Cmah repression caused activation-dependent dynamic reduction of CD22 ligand expression without losing α2,6-linked sialylation in germinal centers. The in vivo function of *Cmah* was analyzed using gene-disrupted mice. Phenotypic analyses showed that Neu5Gc glycan functions as a negative regulator for B-cell activation in assays of T-cell-independent immunization response and splenic B-cell proliferation. Thus, Neu5Gc is required for optimal negative regulation, and the reaction is specifically suppressed in activated B cells, i.e., germinal center B cells.**

The germinal center is a special microenvironment which occurs in secondary lymphoid organs, mainly in response to T-cell-dependent antigen immunization. Mature B cells entering the germinal center edit their immunoglobulin gene through somatic hypermutation and class-switching recombination, differentiating into memory cells and plasma cells (30, 33). The activated B cells during the germinal center reaction in mice can be probed with peanut (*Arachis hypogaea*) lectin, peanut agglutinin (PNA) (8, 37, 46), or a rat monoclonal antibody (MAb), GL7 (5). GL7 was originally reported as a marker for polyclonally activated T and B cells (28) in mice. GL7 stains a subpopulation of T cells (19) and a subpopulation of the large pre-B-cell stage during differentiation in the bone marrow (38). Activated B cells express the GL7 epitope, but mature B cells do not; thus, GL7 serves as a marker for germinal centers in the immunized spleen (18, 41, 52) or lymph nodes, and $GL7^{high}$ B cells have been shown to have higher functional activity for producing antibodies and presenting antigens (5). Despite growing knowledge about the use of this antibody as a marker for lymphocytes in various conditions, the molecular epitope of GL7 is poorly defined to date. In the original article characterizing GL7, Laszlo et al. (28) showed that GL7 could immunoprecipitate a 35-kDa cell surface protein from metabolically labeled activated B cells. However, no other studies have been published on this subject.

In the present study, we found that GL7 recognizes a glycan moiety containing terminal sialic acid (Sia) in both linkage- and modification-dependent manners. Sia is a family of acidic nine-carbon sugars that often occupies the nonreducing terminus of mammalian glycan chains (47), and Sia is essential for early development of mice (49). The localization of Sia-bearing glycan chains on the cell surface makes sialylated molecules seem to be likely targets for various cellular and molecular recognition molecules, such as the mammalian lectins that are abundant in the immune system (61). A family of enzymes, sialyltransferases, is responsible for the formation of the Sia linkage to the underlying glycan chains. To determine the

* Corresponding author. Mailing address: Laboratory of Membrane Biochemistry and Biophysics, Graduate School of Biostudies, Kyoto University, Yoshida-shimoadachi, Sakyo-ku, Kyoto 606-8501, Japan. Phone: 81 75 753 7684. Fax: 81 75 753 7686. E-mail: yasu@pharm.kyoto-u.ac.jp.

‡ Present address: Research Center for Glycobiotechnology, Ritsumeikan University, Kyoto, Japan.

† Supplemental material for this article may be found at http://mcb.asm.org/.

▽ Published ahead of print on 12 February 2007.

linkage specificity of GL7 recognition, we used the gene expression profiles of sialylation-related genes obtained by DNA microarray analysis to screen for a responsible sialyltransferase gene for the biosynthesis of the GL7 determinant.

Apart from the linkage variations, Sia also occurs in various molecular species as a result of modifications at its C-4, C-5, C-7, C-8, and C-9 positions; these modifications are spatially and temporary regulated (60). We also found that the determinant recognition by GL7 is specific to a Sia modification at the C-5 position. In mice, Sia occurs in two main forms with respect to the moiety at the C-5 position: *N*-acetylneuraminic acid (Neu5Ac), which is a precursor form of the diverse Sia family, and its major modified form, *N*-glycolylneuraminic acid (Neu5Gc). The structural difference between Neu5Ac and Neu5Gc is a single oxygen atom in the C-5 position. The modification reaction that produces Neu5Gc is catalyzed at the sugar-nucleotide level in the cytosol by the enzyme CMP-Neu5Ac hydroxylase (Cmah) (24, 53). Cmah determines the cell surface expression ratio of these two Sia species, as the cytosolic Cmah reaction occurs prior to the sialyltransferase reaction, which takes place in the Golgi apparatus during the biosynthesis of glycoconjugates. We found that GL7 recognizes only Neu5Ac-bearing glycans and that the reduction of *Cmah* expression plays a major role in the formation of the GL7 epitope in activated B cells in the germinal center, which was in sharp contrast to the dominant expression of Neu5Gc in mouse lymphocytes.

To examine the in vivo function of Neu5Gc-bearing glycans, we disrupted the *Cmah* gene in mice. *Cmah* disruption is expected to modify the Sia-mediated Sia species-specific recognition event without affecting overall sialylation, which can affect the behavior of the protein in various ways. We primarily focused on the phenotypic consequences of *Cmah* disruption in B cells since Cmah is regulated in B cells, especially in response to activation. *Cmah*-null mice exhibited hyperresponsive B cell phenotypes in assays measuring B-cell functions, i.e., antibody production and proliferation.

## MATERIALS AND METHODS

**Materials.** Most of the materials used were obtained from Wako Chemical (Osaka, Japan) or Nacalai Tesque (Kyoto, Japan). The human immunoglobulin G1 (IgG1)-Fc fusion construct was provided by Paul Crocker and Ajit Varki. The Lec2 cells were provided by Pamela Stanley. The Plat-E cells were provided by Toshio Kitamura. Human B-cell lines were obtained from the Japanese Collection of Research Bioresources.

**Antibodies and lectins.** The antibodies used were as follows: donkey $F(ab')_2$ against mouse IgM (Jackson ImmunoResearch, West Grove, PA); R-phycoerythrin (R-PE)-conjugated anti-mouse B220 (RA3-6B2); R-PE-conjugated goat $F(ab')_2$ anti-human IgG-Fc; R-PE-conjugated streptavidin (CALTAG Laboratories, Burlingame, CA); fluorescein isothiocyanate (FITC)-conjugated and purified GL7; FITC-conjugated anti-mouse B220 (RA3-6B2); R-PE-conjugated anti-mouse I-A/I-E (M5/114.15.2); biotin-conjugated anti-CD22 (Cy34.1) (BD Pharmingen, San Diego, CA); horseradish peroxidase (HRP)-conjugated goat anti-rat IgM; alkaline phosphatase-conjugated isotype-specific goat anti-mouse IgA, IgG1, IgG3, and IgM; unlabeled isotype-specific goat anti-mouse IgA and IgG3; R-PE-conjugated anti-mouse IgM (1B4B1); biotin-conjugated anti-mouse CD22 (2D6) (Southern Biotechnology Associates, AL); anti-mouse polyvalent Igs; HRP-conjugated PT-66 (an antiphosphotyrosine MAb; Sigma, St. Louis, MO); CD90 (Thy1.2) MicroBeads; anti-FITC MicroBeads (Miltenyi Biotec, Bergisch Gladbach, Germany); rabbit anti-mouse CD22 serum (Chemicon, Temecula, CA), HRP-conjugated donkey $F(ab')_2$ anti-rabbit Ig (Amersham Life Science, Buckinghamshire, United Kingdom); antiactin (Santa Cruz Biotechnology, Santa Cruz, CA); HRP-conjugated goat anti-mouse IgG; HRP-conjugated rabbit anti-goat IgG (ZYMED Lab, South San Francisco, CA). Anti-CD22 MAb (Cy34.1) was purified from the culture supernatant of hybridoma Cy34.1 (ATCC). Biotinylated *A. hypogaea* PNA was obtained from HONEN (Tokyo, Japan), and FITC-conjugated *Sambucus sieboldiana* agglutinin (SSA) was obtained from Seikagaku Kogyo (Tokyo, Japan).

**Preparation of Fc fusion proteins of sialoadhesin and CD22.** Recombinant soluble forms of the amino-terminal domains (domains 1 to 3) of mouse sialoadhesin/Siglec-1, mouse CD22/Siglec-2, and human CD22/Siglec-2 fused to the Fc region of human IgG1 (mSn-Fc, mCD22-Fc, and hCD22-Fc, respectively) were produced in stably transfected Lec2 cells, a cell line deficient in protein sialylation. The production of the Siglec (Sia-binding Ig superfamily lectin)-Fc fusion probe in the Lec2 cell line resulted in considerably enhanced binding to the ligand, which allowed the identification of changes in ligand expression. The Siglec-Fc probes were purified from the culture supernatant using protein A-Sepharose columns (Pierce, Rockford, IL).

**Flow cytometry.** Cell labeling was carried out in fluorescence-activated cell sorter buffer (1% bovine serum albumin [BSA] and 0.1% $NaN_3$ in phosphate-buffered saline [PBS]). Data were acquired using a FACScan (Becton Dickinson, Franklin Lakes, NJ) instrument and analyzed using FlowJo software (Tree Star, San Carlos, CA). For comparison with the microarray data, B lymphoma cells ($1 \times 10^5$) were stained with FITC-conjugated GL7 (dilution, 1:100) for 1 h. This staining condition was determined using the criterion that the strongest staining did not reach a plateau. Mean fluorescence intensity (MFI) of GL7 staining was acquired using a FACScan at settings under which unstained control cells gave a signal of around 5 on the FL-1 channel. The mean FL-1 signal of each stained sample was divided by that of the unstained sample to produce the relative staining profiles on flow cytometry to be compared with the cDNA microarray profiles of relative gene expression. For mSn-Fc, mCD22-Fc, and hCD22-Fc staining, these Fc fusion proteins were precomplexed with R-PE-conjugated goat $F(ab')_2$ anti-human IgG.

**Sialidase treatment.** Sialidase treatment was carried out in 100 mM sodium acetate (pH 5.2) for 30 min at room temperature prior to the staining for flow cytometry. Sialidase from *Arthrobacter ureafaciens* (Calbiochem, San Diego, CA) and sialidase from *Salmonella enterica* serovar Typhimurium (Takara, Kusatsu, Japan) were used.

**Immunoblotting with GL7.** The cells were sonicated in detergent-free lysis buffer (25 mM Tris-HCl [pH 7.6], 1 mM dithiothreitol, protease inhibitor cocktail [Nacalai Tesque]). The pellets (membrane fractions) were collected by ultracentrifugation and solubilized in NP-40 lysis buffer (1% Nonidet P-40, 150 mM NaCl, 25 mM HEPES [pH 7.4], protease inhibitor cocktail). The extracts were subjected to immunoblotting with GL7 in the presence or absence of 100 mM Neu5Ac.

**Development of cDNA microarray for glycan-related genes.** The RIKEN Frontier Human Glyco-gene cDNA microarray, version 2, which was spotted by Takara, consisted of 888 genes, which included glycosyltransferase genes and genes related to sugar metabolism, glycan modification, glycan recognition, and lipid metabolism.

**Use of cDNA microarray for identification of glycan-related genes.** $Poly(A)^+$ RNA samples were isolated from mid-log-phase cells using the mTRAP system (Activemotif, Carlsbad, CA) and were quality checked using a Bioanalyzer 2100 (Agilent Technologies, Santa Clara, CA). One microgram of $poly(A)^+$ RNA from the B-cell lines (rRNA contamination subtracted) and universal reference RNA (Clontech, Mountain View, CA) were labeled using a CyScribe first-strand cDNA labeling kit (Amersham). Competitive hybridization was performed on the microarray, and data were obtained using an Affymetrix 428 array scanner. To achieve a fair cross-cell line comparison, we fixed Cy3 as the signal for the universal reference RNA and Cy5 for the RNA from the B-cell lines. Microarray data were background corrected using a smoothing function and then Lowess normalized using linear models for microarray data. This readout was sigma normalized to avoid variation among microarray replicates. Then, the Cy5 signal from the B-cell lines was divided by the Cy3 signal to obtain the relative expression profile for each gene in the six cell lines as expression ratios relative to the universal reference RNA (1, 16, 29, 40). The gene expression profiles were compared with the GL7 staining profiles from flow cytometry. The similarity between the profiles was evaluated with Pearson's correlation coefficient, and probability values (*P* values) were calculated by the correlation coefficient test. For the correlation coefficient test of a sample size of six, a coefficient of 0.81 indicates a statistical significance level of 5%.

**Transfection.** CHO-K1 cells were stably transfected with pIRES (where IRES is internal ribosome entry site) vector (Clontech), either with or without rat cDNA for *St6gal1*. Transfected cells were selected with G418 (1 mg/ml), and multiple stable clones were established.

**Enzyme-linked immunosorbent assay (ELISA).** In 96-well assay plates, GL7 antibody was immobilized in wells coated with the capturing antibody, purified

anti-rat IgM. The wells were washed and incubated with streptavidin-conjugated sugar chain probes (50 μM), prepared as previously reported (65). The captured probes were detected with biotinylated alkaline phosphatase (Vector Laboratories, Burlingame, CA) and *p*-nitrophenyl phosphate by measuring the absorbance at 405 nm.

**Spleen sectioning and immunohistochemistry.** Mice were immunized intraperitoneally with $3 \times 10^8$ sheep red blood cells (SRBC) in 100 μl of saline. Spleens were removed 8 or 10 days after immunization and embedded in Tissue-Tek OCT (22-oxyacalcitriol) compound (Sakura Finetechnical, Tokyo, Japan). Spleen sections were cut at a 6-μm thickness on a cryostat microtome (Leica Geosystems, Heerbrugg, Switzerland), thaw-mounted onto Matsunari adhesive silane-coated slides, and fixed in acetone. After rehydration in Tris-buffered saline and blocking in Tris-buffered saline with 5% BSA and 0.05% Tween 20, the sections were stained with GL7, PNA, or mCD22-Fc precomplexed with R-PE-conjugated anti-human IgG. The stained sections were analyzed under a confocal laser-scanning microscope (Olympus, Tokyo, Japan).

**Magnetic sorting preparation of splenic B-cell-enriched fraction.** B-cell-enriched fractions were obtained by Thy1.2 depletion of splenocytes on a MACS (magnetic cell sorter) depletion column (Miltenyi Biotec). Thy1.2-depleted fractions were stained with B220 to confirm B-cell enrichment. To avoid Neu5Gc contamination in the experimental systems, RPMI 1640 medium (Invitrogen, Carlsbad, CA) containing 10% human serum (Uniglobe, Reseda, CA) or chicken serum (JRH Biosciences, Lenaxa, KS), rather than fetal bovine serum (FBS) (JRH), was used in most of the experiments. In addition, sodium pyruvate (Invitrogen), nonessential amino acids solution (Invitrogen), L-glutamine, and 2-mercaptoethanol were added to the medium.

**Germinal center B-cell analyses.** Splenic B cells from SRBC-immunized mice were incubated with FITC-conjugated GL7 and then with anti-FITC MicroBeads. The labeled cells were collected as germinal center B cells using a MACS LS column (Miltenyi Biotec). The germinal center, nongerminal center, and control (untreated) B cells were lysed by sonication in detergent-free lysis buffer (described above), and the lysates were separated by ultracentrifugation. The supernatant (cytosolic fraction) was used for immunoblotting with anti-Cmah antibody, and the pellet (membrane fraction) was used for the analysis of Sia species by high-pressure liquid chromatography (HPLC). Immunoblotting was performed using rabbit N8 antiserum against mouse Cmah, as previously reported (27). The ratios of Neu5Gc were determined by derivatizing Sia with 1,2-diamino-4,5-methylenedioxybenzene (DMB), a fluorescent compound for α-keto acids, as previously described (27). In brief, Sia was released by incubating the pellet in 2 M acetic acid at 80°C, derivatized with DMB (Dojindo, Mashiki, Japan), and analyzed on a reverse-phase column (TSK-gel ODS-80Tm; Tosoh, Tokyo, Japan) using a Shimadzu LC10 HPLC system.

**Detection of Sia in tissues.** The ratios of Neu5Ac and Neu5Gc were determined as above. Sia was released by incubating tissues in 100 mM sulfuric acid (which also destroys the *O*-acetyl group often found on the C-7 to C-9 positions of Sia molecules), derivatized with DMB, and analyzed by HPLC.

**Real-time RT-PCR analysis.** Real time reverse transcription-PCR (RT-PCR) experiments were performed using a QuantiTect SYBR Green PCR kit (QIAGEN Japan, Tokyo, Japan) and an ABI 7700 sequence detection system (Applied Biosystems Japan, Tokyo, Japan). Total RNA was purified from untreated or lipopolysaccharide (LPS)-stimulated mouse splenic B cells, and 2 μg was used for reverse transcription. The amplification cycle was as follows: 15 min at 95°C, followed by up to 40 cycles of 15 s at 94°C, 30 s at 58°C/50°C, and 30 s at 72°C. The PCR primers used for amplification were: ZP-5, 5′-AGATTTAC AAGGATTCC-3′; ZP-E, 5′-CTTAAATCCAGCCCA-3′ (*Cmah*); PS-mCD22-6, 5′-CCTCCACTCCTCAGGCCAGA-3′; PS-mCD22-E, 5′-GCCTATCCCATTG GTCCCT-3′ (*Cd22*); PS-ST6Gal-1, 5′-TCTTCGAGAAGAATATGGTG-3′; PS-ST6Gal-A, 5′-GACTTATGGAGAAGGATGAG-3′ (*St6gal1*); PS-GAPDH-1 (where GAPDH is glyceraldehyde-3-phosphate dehydrogenase), 5′-GTGGAGATTGTTGCC ATCAACG-3′; PS-GAPDH-A, 5′-TCTCGTGGTTCACACCCATCAC-3′ (*Gapdh*); PS-BACTIN-1, 5′-ACGATATCGCTGCGCTGGTC-3′; and PS-BACTIN-A, 5′-CAT GAGGTAGTCTGTCAGGT C-3′ (*Actb*). Each sample was analyzed in more than three wells. Relative mRNA abundance was calculated using the comparative cycle threshold method and expressed as a ratio to the nonstimulated sample.

**Retrovirus preparation and infection.** *Cmah* cDNA was cloned into the modified mouse stem cell virus vector, which expresses *Cmah* and the extracellular domain of human *CD4* by means of an internal ribosome entry site. Plasmids were transiently transfected into Plat-E packaging cells (35), and retrovirus-containing supernatants were collected. After stimulation with LPS for 12 to 14 h, splenic B cells were spin infected (at 32°C for 90 min) with the retrovirus in the presence of *N*[1-(2,3-dioleoyloxy)propyl]-*N*,*N*,*N*-trimethylammonium methylsulfate (DOTAP; Roche Diagnostics, Mannheim, Germany). The retrovirus-infected B cells were cultured in the presence of 30 μg/ml LPS for 2 to 2.5 days, and then human CD4-positive cells were enriched with a MACS system using MACSelect 4 MicroBeads (Miltenyi Biotec). The sorted cells were subjected to flow cytometry or a proliferation assay (described below).

**Targeting construct and embryonic stem (ES) cells.** The *Cmah* targeting vector was assembled from a 129/Sv genomic clone containing exons 4 and 5 of this gene and a neomycin resistance gene driven by the phosphoglycerate kinase 1 promoter (PGK-neoR) as well as a diphtheria toxin A gene fragment driven by the MC1 promoter (DT-A) as positive and negative selection markers, respectively. The construct was created by inserting the PGK-neoR cassette into the NspV site of exon 5 of the *Cmah* gene. The DT-A cassette was then ligated adjacent to the 3′ terminus of the construct.

**Generation of mutant mice.** Gene targeting and generation of mutant mice were performed essentially as described previously (23). In brief, E14 cells were electroporated with a Bio-Rad Gene Pulser (0.8 kV; 3 μF) using 30 μg of NotI-linearized targeting vector. The electroporated cells were selected in medium containing G418 (125 μg/ml) and screened for homologous recombination by Southern blot analysis of genomic DNA digested with BglI, using both radiolabeled 5′ internal and 3′ external probes. The mutant cells were microinjected into 3.5-day-old C57BL/6J blastocysts, and the embryos were transferred into the uteri of pseudopregnant ICR mice. Mice were used for the determination of immunological features after more than seven backcrosses to the C57BL/6J strain. All mice examined in this study were housed in a specific-pathogen-free facility.

**Serum isotype-specific antibody measurement.** Serum samples from nonimmunized mice at 8 to 12 weeks of age were subjected to isotype-specific ELISAs. Isotype-specific capturing antibodies were coated onto 96-well ELISA plates, and nonspecific binding was blocked with 1% BSA-supplemented PBS. A serially diluted standard MAb of each isotype (Ancell, Bayport, MN) and diluted serum samples were captured on the wells. The captured Abs were detected with alkaline phosphatase-conjugated isotype-specific goat IgG using a 1420 ARVO SXc (Wallac, Turku, Finland) luminometer.

**Determination of antibody production in immunized mice.** Eight-week-old mice were immunized after preimmune serum was obtained. Freund's complete adjuvant containing 100 μg of dinitrophenyl (DNP)-keyhole limpet hemocyanin (KLH) was used for primary T-dependent immunization by intraperitoneal injection, and a second boost was performed with the antigen in incomplete adjuvant. For T-independent immunization, 10 μg of DNP-Ficoll in PBS was injected. The anti-DNP titer was measured essentially as above, except that DNP-BSA was used for antibody capture, and a mixed pool of DNP-KLH-immunized serum was used as the standard. The value relative to that of the pooled serum was used to normalize the values obtained from different plates.

**B-cell proliferation analysis.** In 96-well plates, 100-μl aliquots of B cells at $1 \times 10^5$ cells/ml were stimulated in RPMI 1640 medium containing the indicated concentrations of stimulation reagents. After 24 h of incubation, bromodeoxyuridine (BrdU) was added, and the incubation was continued overnight. Incorporated BrdU was detected using a chemiluminescent ELISA system (Roche Diagnostic GmbH) with an 1420 ARVO SXc luminometer.

**Immunoblotting and immunoprecipitation of CD22.** Splenic B cells were adjusted to $5 \times 10^5$ cells/50 μl in RPMI 1640 medium. After preincubation at 37°C, the B cells were stimulated with $F(ab')_2$ anti-mouse IgM (10 μg per $5 \times 10^5$ cells) at 37°C. To detect the pattern of tyrosine phosphorylation, cells were lysed in sodium dodecyl sulfate-polyacrylamide gel electrophoresis sample buffer (50 mM Tris-HCl [pH 7.6], 2% sodium dodecyl sulfate, 0.1% pyronin G, 10% glycerol, 2-mercaptoethanol). For immunoprecipitation studies, the stimulated B cells were lysed in NP-40 lysis buffer (1% Nonidet P-40, 150 mM NaCl, 25 mM HEPES [pH 7.4], 5 mM NaF, 2 mM sodium orthovanadate, protease inhibitor cocktail [Nacalai Tesque]), and CD22 was immunoprecipitated with anti-CD22 (Cy34.1) antibody and protein G-Sepharose beads (Amersham Biosciences). In the CD22 immunoprecipitation studies, after a probing step with PT-66, the membrane was reprobed with anti-CD22 polyclonal antibody.

**Experimental animals.** The studies presented here were performed in accordance with animal care guidelines and were approved by the animal experimental committee of Kyoto University Graduate School of Biostudies.

**Microarray data accession numbers.** The GEO platform (GPL3465) and experimental results are registered in the Gene Expression Omnibus database under accession number GSE4407.

## RESULTS

**Sia involvement in GL7 staining of B-cell lines.** During B-cell development in mice, the epitope of the MAb GL7 appears and disappears in multiple maturation steps (5, 18, 32,

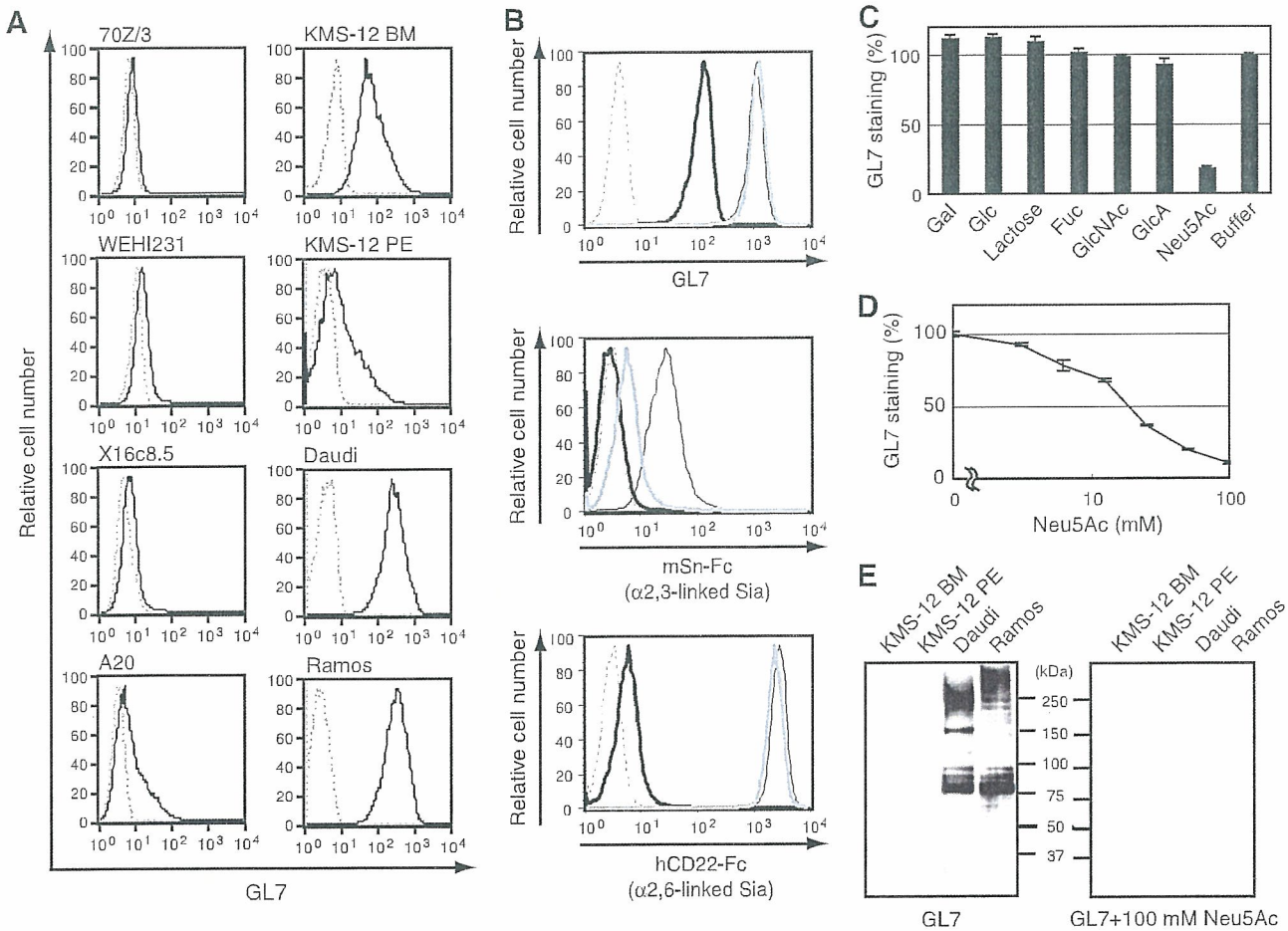


FIG. 1. Involvement of Sia in the GL7 epitope. (A) GL7 staining in flow cytometry. Mouse B-cell lines (70Z/3, WEHI231, X16c8.5, and A20) and human B-cell lines (KMS-12 BM, KMS-12 PE, Daudi, and Ramos) were stained with FITC-conjugated GL7. Black solid lines indicate staining with GL7, and gray dashed lines indicate nonstaining controls. (B) The effect of sialidase treatment on GL7 staining. Daudi cells were treated with sialidase before staining with FITC-conjugated GL7, mSn-Fc, or hCD22-Fc. Gray dashed lines indicate negative controls (nonstaining for GL7 and R-PE-conjugated anti-human IgG for the others), and black thin lines indicate the results without sialidase treatment. Black bold lines indicate the results with *A. ureafaciens* sialidase treatment, and gray bold lines indicate results with *S. enterica* serovar Typhimurium sialidase treatment. Sialidase from *A. ureafaciens* releases α2-3,6,8-linked Sia, whereas sialidase from *S. enterica* serovar Typhimurium is specific to the α2-3 linkage. To confirm the effect of sialidase treatment, changes in cell surface expression of α2,3-linked Sia and α2,6-linked Sia were detected with mSn-Fc and hCD22-Fc chimeric probes precomplexed with R-PE-conjugated anti-human IgG, respectively. (C and D) Effect of free sugars on GL7 binding. Daudi cells were stained with FITC-conjugated GL7 in the presence of 50 mM free sugars (C) or the indicated concentrations of Neu5Ac (D). The data are shown as the relative MFI of each staining. Gal, galactose; Glc, glucose; Fuc, fucose; GlcNAc, *N*-acetylglucosamine; GlcA, glucuronic acid. (E) GL7 blotting of human B-cell lines. Membrane fractions of human B-cell lines (KMS-12 BM, KMS-12 PE, Daudi, and Ramos) were analyzed by GL7 immunoblotting. The addition of 100 mM Neu5Ac during incubation with GL7 reduced most of the staining on blotted membranes.

38). We were interested in the change of GL7 epitope expression, and thus we first assessed the reactivity of this antibody with various B-cell lines, including human germinal center-like Burkitt lymphomas. GL7 showed stronger reactivity toward human B-cell lines than toward mouse B-cell lines (Fig. 1A). The GL7 epitope has been shown to be sensitive to sialidase treatment, although the type of sialidase used in the study reporting this finding was not specified (19). To understand the relationship of GL7 epitopes present on human B-cell lines and mouse activated B cells, we further characterized the determinant on human B-cell lines. The GL7 epitope on Daudi cells was similar to that on mouse activated B cells, as GL7 staining of Daudi cells was also inhibited by sialidase treatment when a broad-range sialidase, *A. ureafaciens* sialidase, was used (Fig. 1B). In contrast, *S. enterica* serovar Typhimurium sialidase, which is specific to α2,3-linked Sia, had no effect (Fig. 1B). To assess the role of Sia and other sugars in GL7 reactivity, we analyzed the inhibitory effects of sugar on GL7 binding. The results clearly showed specificity of Neu5Ac for inhibition (Fig. 1C), and the inhibition was dependent on the Neu5Ac concentration (Fig. 1D). Neu5Ac is a major form of Sia in human cells. GL7 binding was decreased with a metabolic N-glycosylation inhibitor, tunicamycin (see Fig. S1 in the supplemental material). Multiple bands were detected in immunoblotting experiments using the membrane fraction of Daudi cells (Fig. 1E). Thus, it is likely that GL7 recognizes some glycan epitopes, including Sia, rather than some specific protein(s).

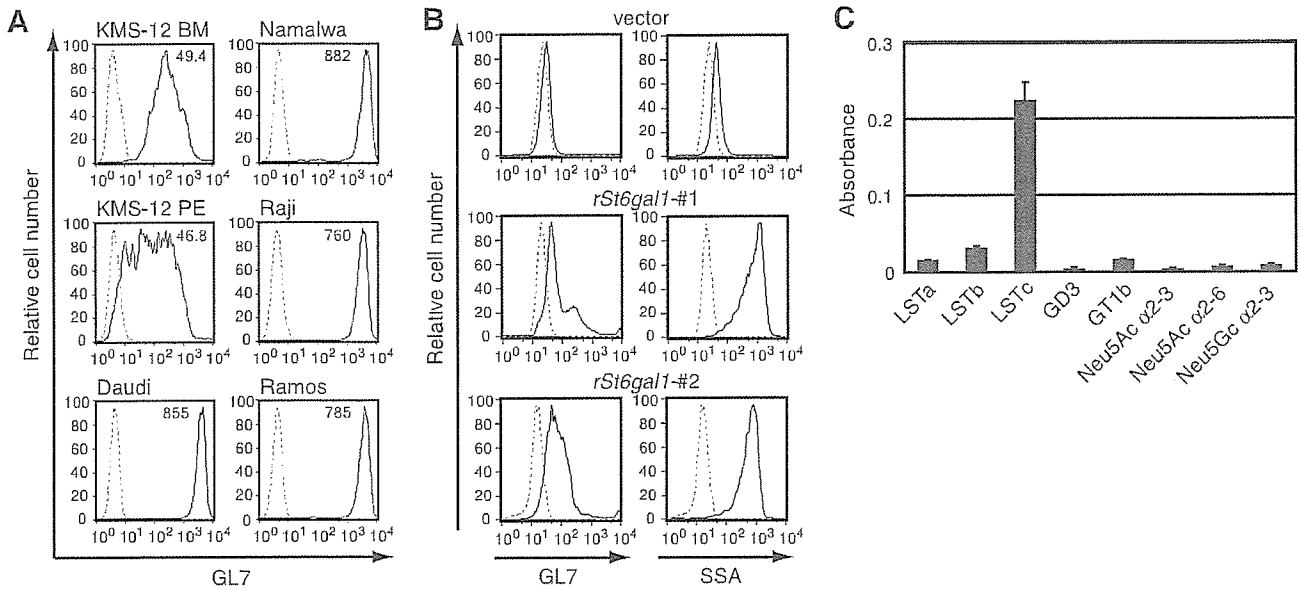


FIG. 2. Involvement of α2,6-linked Neu5Ac in the GL7 epitope. (A) Numerical comparison of GL7 staining among human B-cell lines. The results of GL7 staining of human B-cell lines were numerically compared using MFI values in flow cytometry. To normalize the binding in different cells, the endogenous fluorescence of sample cells (gray dashed lines) was adjusted to an MFI of around 5. For comparison with the gene expression profile, GL7-stained MFI values were divided by the background value. The relative values indicated on the top of each staining were used as the GL7 determinant expression profile. (B) Appearance of the GL7 determinant by ST6GAL1 expression. CHO-K1 clones stably transfected with rat *St6gal1* or an empty vector (as a control) were stained with FITC-conjugated GL7 or FITC-conjugated SSA. The results from two such clones are shown. (C) Carbohydrate binding assay of GL7. Carbohydrate binding was measured using ELISA. Data are shown as the means of triplicate samples, and the bars represent standard errors of the mean. LSTa, Neu5Acα2-3Galβ1-3GlcNAcβ1-3Galβ1-4Glc; LSTb, Galβ1-3(Neu5Acα2-6)GlcNAcβ1-3Galβ1-4Glc; LSTc, Neu5Acα2-6Galβ1-4GlcNAcβ1-3Galβ1-4Glc; GD3, Neu5Acα2-8Neu5Acα2-3Galβ1-4Glc; GT1b, Neu5Acα2-3Galβ1-3GalNAcβ1-4(Neu5Acα2-8Neu5Acα2-3)Galβ1-4Glc; Neu5Ac α2-3, Neu5Acα2-3Galβ1-4Glc; Neu5Ac α2-6, Neu5Acα2-6Galβ1-4Glc; Neu5Gc α2-3, Neu5Gcα2-3Galβ1-4Glc.

**Strong correlation between expression of the GL7 epitope and expression of the *ST6GAL1* gene in human B-cell lines.** Sia clearly plays an important role in GL7 epitope expression. Interestingly, the GL7 staining of a panel of human B-cell lines was not uniform but, instead, exhibited different intensities (Fig. 1A). Given that a number of bands were detected in immunoblotting experiments, the differences in GL7 epitope expression seemed to be caused by differences in the expression level of an enzyme(s) involved in the biosynthesis of the GL7 epitope glycan rather than differences in carrier protein expression. Therefore, we analyzed the correlation of GL7 epitope expression with the relative level of Sia-related gene expression. The reason to expect such a correlation was that glycosyltransferase activity tends to be regulated through the control of gene expression and substrate accessibility rather than through posttranslational modifications. Six human B-cell lines were stained with GL7 (Fig. 2A), and the relative MFI from flow cytometry was compared with the gene expression profile of the same set of B-cell lines obtained from a newly developed cDNA microarray that can be used to analyze the expression of glycan-related genes. To perform cross-sample comparisons of gene expression among cell lines, we compared poly(A)$^+$ RNA from each B-cell line and commercially available universal reference RNA. The relative gene expression was obtained by dividing the cDNA microarray fluorescence signal from cellular RNA by that of the universal reference (see Table S1 in the supplemental material). From among the genes spotted on the microarray, various genes for sialyltransferases and Sia-metabolizing enzymes were picked to examine their possible relationships to the degree of GL7 staining, because it has been shown that sialyltransferase gene expression might correlate with the surface phenotype of lectin binding (2). We calculated the Pearson's correlation coefficient. Among the sialyltransferase and other Sia-metabolizing enzyme genes, *ST6GAL1* showed the strongest correlation between its expression profile and the GL7 staining profile (Table 1). This result indicates that *ST6GAL1* expression could be responsible for the biosynthesis of the GL7 epitope in these human B-cell lines. ST6GAL1 transfers Sia onto a Gal residue of terminal *N*-acetyllactosamine (LacNAc; Gal β1-4GlcNAc) with an α2,6 linkage (42), and B cells have been shown to express this enzyme (20, 64). This indicates that the terminal transferase reaction by ST6GAL1, but not the supply of the substrate, is the rate-limiting step in GL7 epitope biosynthesis in these cells. Interestingly, a negative correlation was found between GL7 staining and the expression of *SIAE*, a gene encoding Sia 9-*O*-acetylesterase (Table 1). Although Sia 9-*O*-acetylesterase cleaves the *O*-acetyl group of Sia, *SIAE* is expressed in cell types expressing its substrate, 9-O-acetylated Sia (57). If the degree of 9-O acetylation were to correspond with the level of *SIAE* expression, GL7 binding might be negatively affected by 9-*O*-acetyl modification, similar to CD22 (56).

**Effect of ST6GAL1 overexpression on GL7 epitope expression.** Data from the correlation index calculation suggest that GL7 recognizes α2,6-linked Sia on N-glycan and that the expression of the GL7 epitope on human B cells depends mainly

TABLE 1. Pearson's correlation index analysis of Sia-related genes[a]

| Index | *P* value | Gene name | Encoded enzyme |
|---|---|---|---|
| 0.937 | 5.87E-3 | *ST6GAL1* | ST6Gal I |
| 0.806 | 5.30E-2 | *ST3GAL3* | ST3Gal III |
| 0.551 | 2.57E-1 | *CMAH* | Pseudogene for CMP-Neu5Ac hydroxylase |
| 0.473 | 3.44E-1 | *ST3GAL2* | ST3Gal II |
| 0.215 | 6.82E-1 | *SLC35A1* | CMP-Sia transporter |
| 0.173 | 7.43E-1 | *ST8SIA1* | ST8Sia I |
| 0.142 | 7.89E-1 | *ST3GAL6* | ST3Gal VI |
| 0.137 | 7.96E-1 | *PGM3* | GlcNAc-6-P mutase |
| 0.096 | 8.56E-1 | *GMPPB* | GDP-Man pyrophosphorylase |
| 0.052 | 9.22E-1 | *ST6GALNAC2* | ST6GalNAc II |
| −0.103 | 8.47E-1 | *ST8SIA3* | ST8Sia III |
| −0.196 | 7.10E-1 | *ST8SIA4* | ST8Sia IV/PST |
| −0.210 | 6.89E-1 | *GNE* | UDP-GlcNAc-2-epimerase/ ManNAc kinase |
| −0.283 | 5.87E-1 | *ST6GALNAC6* | ST6GalNAc VI |
| −0.442 | 3.80E-1 | *ST3GAL5* | ST3Gal V |
| −0.448 | 3.72E-1 | *ST6GALNAC1* | ST6GalNAc I |
| −0.452 | 3.68E-1 | *ST8SIA5* | ST8Sia V |
| −0.508 | 3.04E-1 | *SAS* | Neu5Ac-9-P synthase |
| −0.639 | 1.72E-1 | *ST6GALNAC4* | ST6GalNAc IV |
| −0.678 | 1.39E-1 | *NEU3* | Membrane sialidase |
| −0.696 | 1.25E-1 | *NEU1* | Lysosomal sialidase |
| −0.739 | 9.30E-2 | *ST8SIA2* | ST8Sia II/STX |
| −0.742 | 9.12E-2 | *ST3GAL4* | ST3Gal IV |
| −0.898 | 1.52E-2 | *ST3GAL1* | ST3Gal I |
| −0.938 | 5.62E-3 | *SIAE* | Sia-9-*O*-acetylesterase |

[a] Pearson's correlation coefficient (index) values of relative gene expression in the microarray against relative GL7 staining MFI among six B-cell lines were calculated for sialyltransferase genes and Sia metabolism-related genes. A positive value indicates the presence of a correlation between gene expression and staining. A negative value indicates the presence of a negative correlation. Index values are also expressed as *P* values.

on *ST6GAL1* expression. To evaluate these findings, we explored the ST6GAL1 expression dependence of GL7 epitope expression. CHO-K1 cells are known to lack α2,6-linked Sia on their cell surfaces. As expected, the parental CHO-K1 cells were GL7 negative (data not shown), as were vector-transfected CHO-K1 cells (Fig. 2B). In contrast, rat *ST6GAL1* (r*St6gal1*)-transfected CHO-K1 cells showed a marked increase in GL7 staining (Fig. 2B). The increase in GL7 staining upon r*St6gal1* expression coincided with the increase in staining by SSA, a plant lectin which reacts with Sia α2,6-Gal/GalNAc on glycans. As CHO-K1 cells are nonimmune cells, GL7 seemed to recognize α2,6-linked Neu5Ac-containing sugar chains on various proteins. Immunoblotting analysis of these stable clones further clarified that the introduction of r*St6gal1* was sufficient to give rise to bands on the blot. The membrane fractions of both CHO-K1 stable clones and human B-cell lines resulted in multiple bands (data not shown).

**Glycan-binding assay of GL7.** To confirm that GL7 is an antiglycan antibody that recognizes α2,6-linked Sia and also to determine the fine specificity of the epitope, we examined GL7 binding to various glycan probes (65) by ELISA. GL7 bound to LSTc (Neu5Acα2-6Galβ1-4GlcNAcβ1-3Galβ1-4Glc) but not to its structural isomer with α2–3 linked Neu5Ac, LSTa (Neu5Acα2-3Galβ1-3GlcNAcβ1-3Galβ1-4Glc) (Fig. 2C). Interestingly, GL7 did not bind to Neu5Acα2-6Galβ1-4Glc (sialyllactose) in spite of the existence of α2,6-linked Neu5Ac in the probe. The glucose (Glc) of the reducing terminal was destroyed during probe preparation for coupling with streptavidin. Thus, it is likely that the structure of Neu5Acα2-6Gal is not sufficient for GL7 binding but that the binding requires at least a trisaccharide for optimal recognition or GlcNAc in the underlying lactosamine. Taking all of the results into consideration, we concluded that GL7 recognizes α2,6-linked Sia-containing glycan chains that are often found on N-glycans of various proteins.

**A shift in the major Sia species, Neu5Gc to Neu5Ac, in the mouse germinal center reaction.** It was still not clear why GL7 failed to react with mouse mature B cells, given that these cells abundantly express α2,6-linked sialoglycans, as St6gal1 is also expressed in these cells (20, 64). The dominant difference in sialylation between mice and humans occurs in the Sia modification at the C-5 position (60). Humans predominantly express Neu5Ac, whereas the major Sia in mice is Neu5Gc (Fig. 3A). It is possible that the change in GL7 reactivity could be a consequence of the change in sia modification. Neu5Gc modification in biosynthesis is regulated by the Cmah reaction in the cytosol, which metabolically gives rise to the donor, CMP-Neu5Gc, for a subsequent sialyltransferase reaction(s) in the Golgi apparatus (Fig. 3B) (24, 25). We therefore asked whether mouse B cells undergo a change in Sia species, from Neu5Gc to Neu5Ac, in GL7-positive cells. We first stained the germinal centers with GL7 and the lectin domain of mouse CD22 (mCD22-Fc), because mouse CD22 demonstrates a marked preference for Neu5Gc-bearing over Neu5Ac-bearing α2,6-linked sialoglycan ligands (26, 44, 50). As shown in Fig. 3C, in the SRBC-immunized mouse spleen, GL7-positive germinal centers were specifically excluded by mCD22-Fc recognition. This complementarity of staining appeared to be the result of the probe preferences, Neu5Ac for GL7 and Neu5Gc for mCD22-Fc, respectively. We then assessed Cmah expression and the Neu5Ac-Neu5Gc ratio in GL7-positive germinal center B cells. Germinal center (GL7-bound) cells showed severely reduced expression of Cmah, and this reduction coincided with the loss of Neu5Gc in the membrane fraction of the cells (Fig. 3D). In contrast, GL7-negative SRBC-immunized B cells were not significantly different from nonimmunized splenic B cells. Thus, the gain of GL7 staining reflected the loss of the CD22 ligand in germinal center B cells due to the repression of Cmah.

**Real-time PCR analysis during mouse B cell activation.** LPS stimulation induces the GL7 epitope in B cells (28). Therefore, we adopted this system to assess the enzyme (gene) responsible for GL7 epitope expression. Cmah is responsible for Sia species change, and St6Gal1 is responsible for Sia linkage biosynthesis. We examined the expression of *Cmah* and *St6gal1* to determine whether changes in the expression of these genes could account for the GL7 epitope induction detected in B-cell activation events. In real-time RT-PCR experiments, *Cmah* expression showed an 80% reduction in LPS-stimulated B cells compared with unstimulated splenic B cells after 48 h of incubation (Fig. 4A). This reduction was already detectable after 3 h of culture. Despite the slightly enhanced expression level of α2,6-linked Sia-containing glycan probed with SSA, *St6gal1* expression showed a subtle reduction in activated B cells after 48 h (Fig. 4A and B). *Cmah* reduction appears to play a prominent role in the appearance of the GL7 epitope in activated B cells. Retrovirus-mediated ectopic *Cmah* expression consistently reduced the expression of the GL7 epitope in